JOURNAL OF AIRCRAFT
Vol. 45, No. 2, March–April 2008

Numerical Simulation of Surface Heat Transfer from an Array of Hot-Air Jets

Farooq Saeed*
King Fahd University of Petroleum and Minerals, Dhahran 31261, Saudi Arabia

DOI: 10.2514/1.33489

A numerical study was conducted to simulate the heat transfer from an array of jets onto an impingement surface typical of those found on aircraft wing/slat surfaces. The study used the commercially available computational fluid dynamics software FLUENT to model the different hot-jet arrangements that included 1) a single array of jets, 2) two staggered arrays of jets at different stagger angles (10 and 20 degrees), and 3) a case with an etched surface. The main findings of the study reveal that the single array and the array with a 20 degree stagger yield better surface heat transfer than the 10 degree stagger. The etched surface or inner liner yields almost 2–3 times better surface heat transfer than the others, thus making it a favorable choice for increasing surface heat transfer.

Nomenclature

A	=	surface area or reference area based on hole diameter, m^2
a	=	piccolo tube diameter, 0.5 m
c_n	=	spanwise distance between holes or spanwise hole spacing, 0.15 m
D	=	diameter of impingement wall semicylinder, 0.75 m
d	=	jet hole diameter, 0.025 m
d_n	=	jet-to-jet slant distance taking into account the stagger
h_c	=	local convection heat-transfer coefficient, $W/m^2 \cdot K$
h_n	=	jet exit height, m
k	=	thermal conductivity or air, $W/m \cdot K$
k_w	=	thermal conductivity of impingement wall (aluminum), $W/m \cdot K$
L_{ref}	=	reference length, 0.0025 m
M	=	jet Mach number
$\dot{m}$	=	mass flow rate, $\rho A v_{av}$, kg/s
Nu	=	Nusselt number, $h_c L_{ref}/k$
p	=	pressure, Pa
q	=	convective heat flux, $h_c(T_w - T_{ref})$, W/m^2
$\dot{q}$	=	heat-transfer rate, W
$\bar{q}$	=	area-weighted average of total surface heat flux through the impingement wall, W/m^2
Re	=	Reynolds number based on jet hole diameter (three-dimensional), $\rho v_{av} d/\mu$
Re_S	=	Reynolds number based on jet slot width (two-dimensional), $\rho v_{av} S/\mu$
S	=	jet slot width, m
s	=	impingement surface arc length, m
T	=	temperature, K
T_{jet}	=	hot-air jet temperature, K
T_{ref}	=	reference temperature, 288 K
T_w	=	impingement wall temperature, 260 K
u_τ	=	shear/friction velocity, $(\tau_w/\rho_w)^{0.5}$, m/s
v_{av}	=	average jet velocity (also V_{jet}), m/s
y^+	=	nondimensional distance, $\rho u_\tau y_p/\mu$
y_p	=	height of point P (first cell center adjacent to wall), m
z_n	=	radial distance between hole and the impingement wall, 0.125 m
θ	=	jet angle measured from the horizontal, deg
μ	=	viscosity, $kg/m \cdot s$
μ_{ref}	=	reference viscosity, 1.7894×10^{-5} $kg/m \cdot s$
ρ	=	density, kg/m^3
ρ_{ref}	=	reference density, 1.225 kg/m^3
τ_w	=	shear stress, N/m^2

Subscripts

anti	=	anti-icing related value
ref	=	reference value
w	=	wall

I. Introduction

AIRCRAFT manufacturers are facing ever-increasing demands to improve safety and performance and to reduce noise, weight, fuel burn, and costs. Many of these parameters are mutually exclusive, resulting in the need to conduct tradeoff studies to determine the optimum design for cost, which demands a high degree of specialist knowledge in several areas of aeronautical engineering. A wing is a major component of any aircraft and houses several internal and external systems: ailerons, flaps, air brakes, fuel, anti-icing, etc. To enhance flight safety under natural icing conditions, one of the several key tasks outlined in the Federal Aviation Administration (FAA) In-Flight Aircraft Icing Plan [1,2] is to ensure the validity and reliability of icing and anti-icing simulation methods currently being used for aircraft performance evaluation and certification.

The anti-icing system most commonly used on commercial aircraft is the hot-air anti-icing system (Fig. 1a). The hot-air anti-icing system uses hot air from the engine compressor bleed to eliminate ice accreting on critical wing surfaces such as the slat (Fig. 1b). A system of external mounted ice detectors with a sensing probe oscillating with a set frequency, which decreases as ice accumulates on the surface, acts as a warning system. The acquisition of improved and innovative techniques, together with the necessary databases on key technologies, will enhance the ability of aircraft manufacturers to introduce safer and radically improved wing designs to the marketplace. This study addresses a key technology, namely ice and rain protection. The main aim of the study is to develop an understanding of the fluid mechanics and heat-transfer process in an anti-icing system with a view to optimize its performance and reduce its weight and cost.

For an aircraft to meet safety regulations as well as certification requirements for flight into icing conditions, it must be protected against impact damage and performance degradation effects due to the strong influence of the wing aerodynamics. Lift can be reduced

Presented as Paper 4287 at the AIAA 25th Applied Aerodynamics Conference, Hyatt Regency, Miami, FL, 25–28 June 2007; received 16 July 2007; revision received 11 September 2007; accepted for publication 27 September 2007.

*Assistant Professor, Aerospace Engineering Department, Mail Box 1637. Member AIAA.

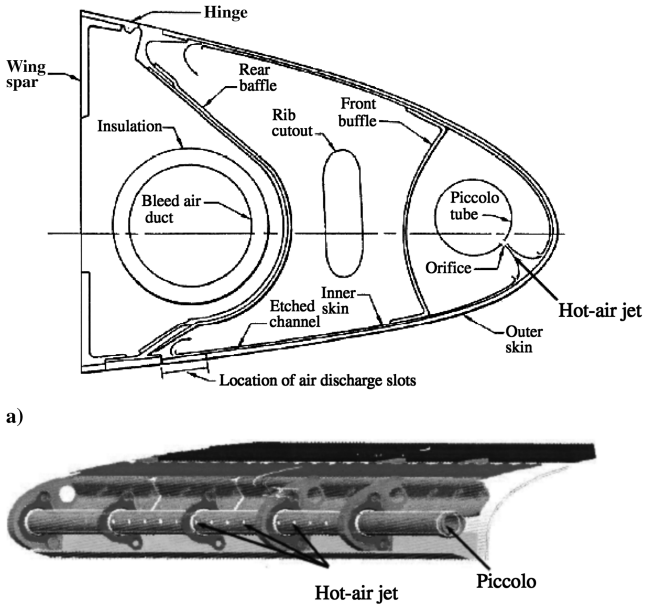

Fig. 1 Internal layout of the piccolo tube inside a) a typical wing leading edge and b) a typical slat (courtesy of Bombardier Aerospace).

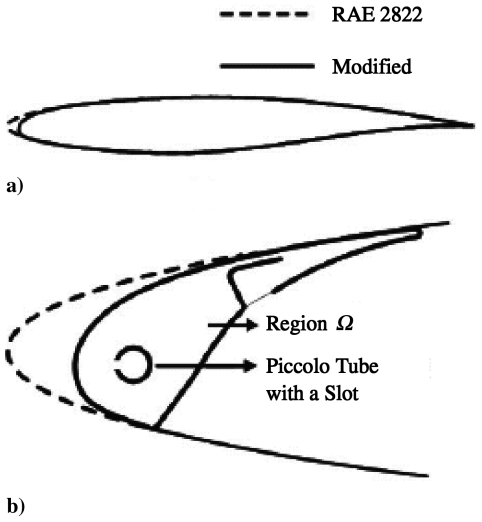

Fig. 2 Typical multi-element airfoil model: a) RAE 2822 airfoil with a modified leading edge to incorporate b) a typical slat.

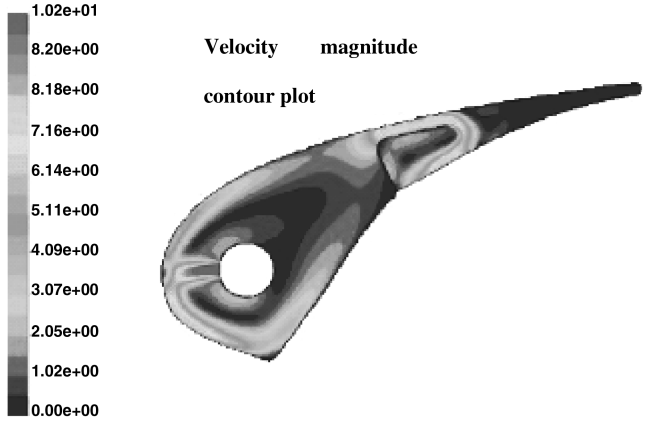

Fig. 3 Numerical simulation of a hot-air jet impingement inside a slat.

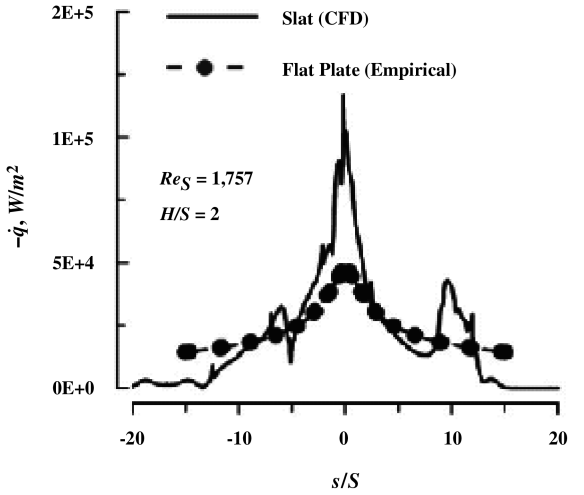

Fig. 4 Comparison of the heat flux distribution $\dot{q}$ on the surface of a slat and a flat plate for a jet Reynolds number $Re_S = 1757$ (H/S= jet height-to-width ratio, s/S = nondimensional surface arc length).

dramatically in conjunction with a very large increase of the drag. The requirements for wing and engine installation on an aircraft, as set out in the relevant Federal Aviation Regulations (FAR) and Joint Airworthiness Requirements (JAR), are typically met by providing the forward lip skin of each vital control surface with a hot-air anti-icing system (Fig. 1a). A hot-air system ensures that even a minimum thickness of ice can be removed from the external surface, a performance that cannot be reached with a pneumatic boot system. Other systems present some limitations in the form of performance

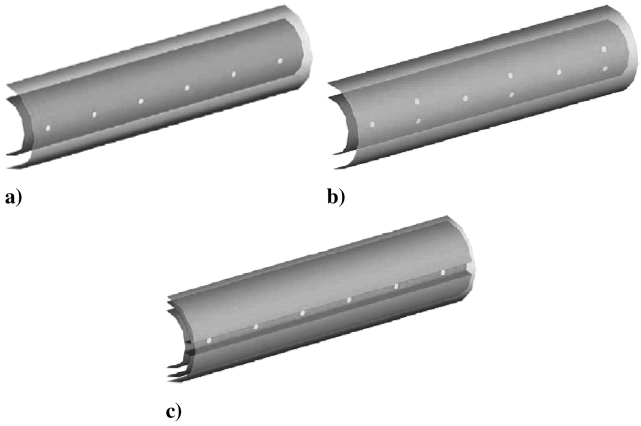

Fig. 5 Different hot-air jet arrangements used in the numerical study: a) an array of single jets, b) an array of staggered jets, and c) an array of single jets and the use baffles and etched channel/liner to enhance heat transfer through the outer surface.

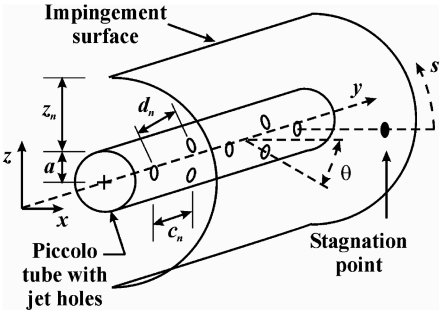

Fig. 6 Geometric parameters used in the study.

Table 1 Description of cases covered in the study

Case no.	Array type	V, m/s	T, K	z_n, m	c_n, m	Stagger θ, deg	h_n, m	d_n, m	Re_{jet}
1	single	200	450	0.125	0.15	0	0.000	0.150	149402
2	staggered	200	450	0.125	0.15	10	0.044	0.156	149402
3	staggered	200	450	0.125	0.15	20	0.087	0.173	149402
4	single	300	450	0.125	0.15	0	0.000	0.150	224102
5	staggered	300	450	0.125	0.15	10	0.044	0.156	224102
6	staggered	300	450	0.125	0.15	20	0.087	0.173	224102
7	single	400	450	0.125	0.15	0	0.000	0.150	298803
8	staggered	400	450	0.125	0.15	10	0.044	0.156	298803
9	staggered	400	450	0.125	0.15	20	0.087	0.173	298803
10	single	200	350	0.125	0.15	0	0.000	0.150	230048
11	single	400	350	0.125	0.15	0	0.000	0.150	460096
12	staggered	400	350	0.125	0.15	10	0.044	0.156	460096
13	staggered	400	350	0.125	0.15	20	0.087	0.173	460096
14	single/liner	200	450	0.125	0.10	0	0.000	0.100	149402
15	single/liner	300	450	0.125	0.10	0	0.000	0.100	224102
16	single/liner	400	450	0.125	0.10	0	0.000	0.100	298803
17	single/liner	200	350	0.125	0.10	0	0.000	0.100	230048
18	single/liner	400	350	0.125	0.10	0	0.000	0.100	460096

Table 2 Summary of mass flow and heat-transfer rates obtained after solution convergence

		Mass flow rate			Heat-transfer rate			
Case no.	Array type	Jet #1, kg/s	Jet #2, kg/s	Exit, kg/s	Jet #1, W	Jet #2, W	Exit, W	Wall, W
1	single	1.897E − 02	1.897E − 02	−3.793E − 02	2.914E + 03	2.914E + 03	−2.317E + 03	−3.510E + 03
2	staggered	1.897E − 02	3.793E − 02	−5.690E − 02	2.914E + 03	5.827E + 03	−3.691E + 03	−5.050E + 03
3	staggered	1.897E − 02	3.793E − 02	−5.690E − 02	2.914E + 03	5.827E + 03	−3.347E + 03	−5.394E + 03
4	single	2.845E − 02	2.845E − 02	−5.690E − 02	4.370E + 03	4.370E + 03	−3.641E + 03	−5.099E + 03
5	staggered	2.845E − 02	5.690E − 02	−8.535E − 02	4.370E + 03	8.740E + 03	−5.862E + 03	−7.249E + 03
6	staggered	2.845E − 02	5.690E − 02	−8.535E − 02	4.370E + 03	8.740E + 03	−5.279E + 03	−7.832E + 03
7	single	3.793E − 02	3.793E − 02	−7.587E − 02	5.827E + 03	5.827E + 03	−5.118E + 03	−6.536E + 03
8	staggered	3.793E − 02	7.587E − 02	−1.138E − 01	5.827E + 03	1.165E + 04	−8.149E + 03	−9.332E + 03
9	staggered	3.793E − 02	7.587E − 02	−1.138E − 01	5.827E + 03	1.165E + 04	−7.412E + 03	−1.007E + 04
10	single	2.438E − 02	2.438E − 02	−4.876E − 02	1.272E + 03	1.272E + 03	−6.523E + 02	−1.892E + 03
11	single	4.876E − 02	4.876E − 02	−9.753E − 02	2.543E + 03	2.543E + 03	−1.465E + 03	−3.622E + 03
12	staggered	4.876E − 02	9.753E − 02	−1.463E − 01	2.543E + 03	5.087E + 03	−2.547E + 03	−5.084E + 03
13	staggered	4.876E − 02	9.753E − 02	−1.463E − 01	2.543E + 03	5.087E + 03	−2.179E + 03	−5.451E + 03
14	single/liner	1.919E − 02		−1.919E − 02	2.947E + 03		−1.749E + 03	−1.198E + 03
15	single/liner	2.878E − 02		−2.878E − 02	4.421E + 03		−2.619E + 03	−1.802E + 03
16	single/liner	3.838E − 02		−3.838E − 02	5.895E + 03		−3.446E + 03	−2.449E + 03
17	single/liner	2.467E − 02		−2.467E − 02	1.287E + 03		−6.340E + 02	−6.525E + 02
18	single/liner	4.933E − 02		−4.933E − 02	2.573E + 03		−1.122E + 03	−1.451E + 03

Table 3 Percentage distribution of heat flux obtained after solution convergence

		Percentage distribution of heat flux		Area-weighted average	Area-weighted average corrected for same heat influx
Case no.	Array type	q_w/q_{in}	$q_{\text{out}}/q_{\text{in}}$	$(\text{W/m}^2)(\text{m}^2)$	$(\text{W/m}^2)(\text{m}^2)$
1	single	60.24%	39.76%	−4.0006E + 04	−6.0008E + 04
2	staggered	57.77%	42.23%	−5.7460E + 04	−5.7460E + 04
3	staggered	61.71%	38.29%	−6.2484E + 04	−6.2484E + 04
4	single	58.34%	41.66%	−5.8455E + 04	−8.7682E + 04
5	staggered	55.29%	44.71%	−8.2064E + 04	−8.2064E + 04
6	staggered	59.73%	40.27%	−8.8587E + 04	−8.8587E + 04
7	single	56.09%	43.91%	−7.4371E + 04	−1.1156E + 05
8	staggered	53.39%	46.61%	1.0568E + 05	1.0568E + 05
9	staggered	57.60%	42.40%	−1.1416E + 05	−1.1416E + 05
10	single	74.36%	25.64%	−2.2099E + 04	−3.3149E + 04
11	single	71.21%	28.79%	−4.1847E + 04	−6.2771E + 04
12	staggered	66.62%	33.38%	−5.8544E + 04	−5.8544E + 04
13	staggered	71.44%	28.56%	−6.2585E + 04	−6.2585E + 04
14	single/liner	40.66%	59.34%	−1.0443E + 05	−2.0645E + 05
15	single/liner	40.76%	59.24%	−1.5371E + 05	−3.0388E + 05
16	single/liner	41.55%	58.45%	−1.9977E + 05	−3.9495E + 05
17	single/liner	50.72%	49.28%	−5.7493E + 04	−1.1366E + 05
18	single/liner	56.39%	43.61%	−1.1105E + 05	−2.1955E + 05

and energy cost [3]. The general principle of the hot-air system is that it takes high-temperature air from the engine compressor and directs it forward onto the inner lip skin surface and, in turn, evaporates impinging water or melts accreted ice on the outer side of the skin, finally limiting the formation of ice. A preferred method of directing the hot air onto the inside skin of the forward lip skin is through the use of a piccolo tube, as shown in Fig. 1, though other methods, having varying degrees of effectiveness, may be used. The piccolo system uses the effect of multiple steady hot jets impinging on the surface and interacting in various ways, thereby heating quite efficiently the inner surface.

The design and assessment of the performance of an anti-icing system at a given flight condition requires reductions of the bleed air mass flow rate, the temperature drop between the engine compressor bleed port and the piccolo ring, and the amount and extent of water caught on the nacelle surface. A thermal balance at the surface is achieved based on forced convective and evaporative cooling, due to the impinging water and forced convective heating due to the piccolo jets. Determination of accurate heat-transfer coefficients is, in general, a complex task, which is considered even more complex for multiple jets impinging on a curved surface. A recent experimental work [4] on this topic indicates that there is still a high degree of conservatism embodied in the thermal analysis associated with anti-icing system design. Thus, there is considerable scope for improving the design of such systems, particularly in the manner in which heat is transferred to the lip skin, and at the same time optimizing the operational benefits.

The wide use of hot-air jets to enhance heat transfer has led to many studies of the flow and heat-transfer characteristics of jet impingement. Jet impingement is used both as a cooling method or heating method in many industrial applications (electronics, chemical processes, etc.). Extensive literature [5,6] on hot/cold-air jet impingement on flat surfaces is available today that addresses key issues such as the effects of jet diameter, orientation, Reynolds number, jet nozzle-to-nozzle distribution, and jet nozzle-to-surface spacing on flow, and heat transfer on flat plates. The flat-plate arena has been thoroughly investigated and empirical relations have been developed that address the aforementioned key issues. However, it is very rare to find studies that have been dedicated to more complex situations such as the interaction of an impingement jet and a curved surface [7]. A few studies that do take into consideration a highly curved impingement surface are mostly restricted to cold-air jet impingement on highly curved surfaces for the study of turbine-blade cooling [8]. Literature on hot-air jet impingement on highly curved surfaces is very scarce [9] and oftentimes the data are proprietary [4]. In fact, there is a lack of literature on experimental and numerical parametric studies of maximum heat transfer from single or multiple hot-air jets impingement on highly curved surfaces that addresses issues such as 1) optimum jet diameter, orientation, and/or jet Reynolds number, 2) optimum jet nozzle-to-surface spacing, 3) optimum number of jets, separation distance between jets, and/or jet nozzle-to-nozzle distribution/arrangement, 4) effect of nozzle geometry, surface curvature, crossflow, and/or turbulence intensity. The absence of such studies, as well as an experimental database, is a

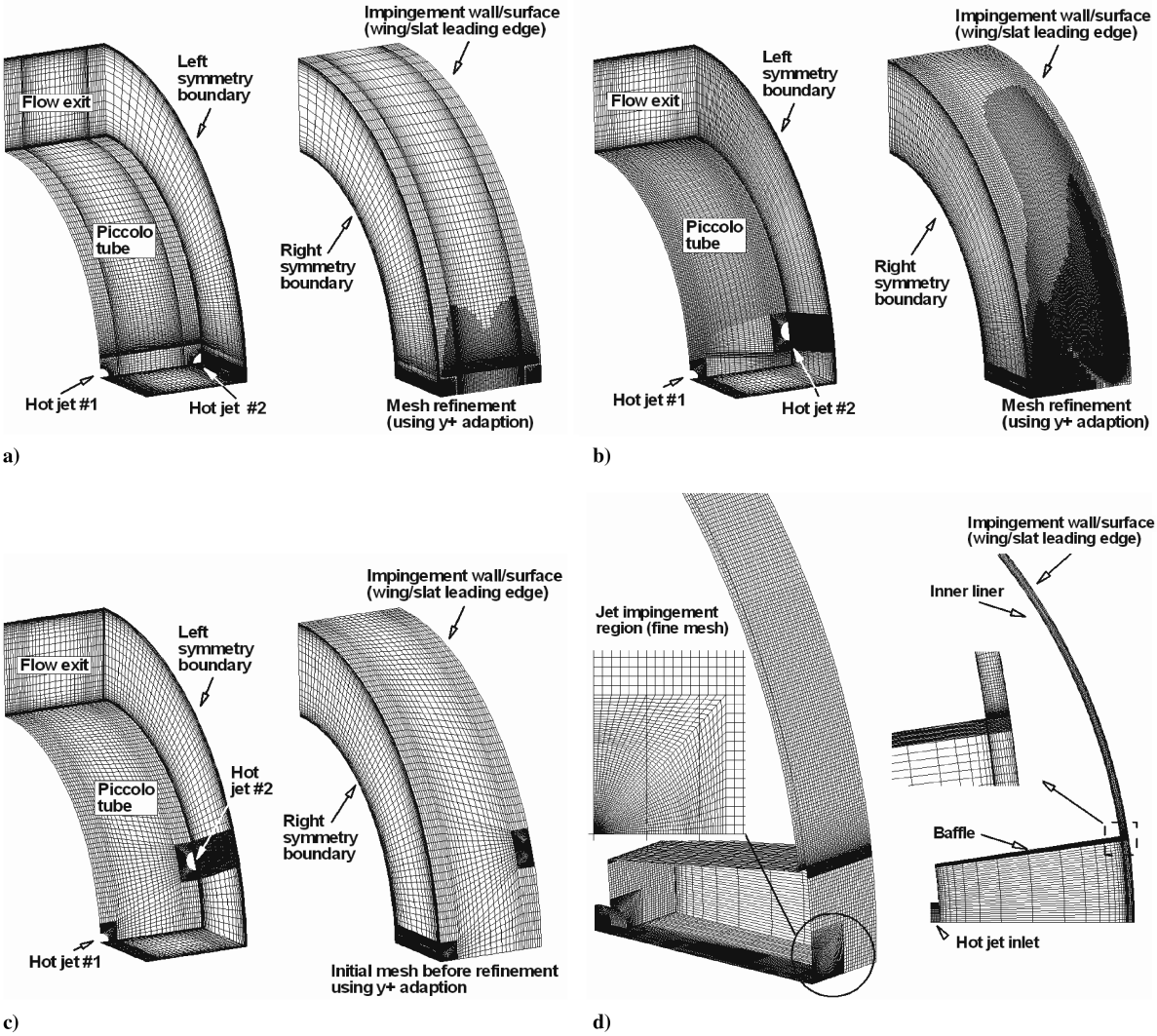

Fig. 7 Grid geometry for the four different configurations.

severe limitation in the design of aircraft anti-icing systems, let alone optimum design of such a system.

In an effort to support the objectives of the FAA Icing Plan and facilitate aircraft manufacturers in the certification process, the main focus of the current research is to reliably simulate a hot-air anti-icing system typical of those in use in commercial aircraft. Presently, a very basic model for a hot-air anti-icing system is employed for such simulations. In this basic model, hot air from the engine is assumed to impinge upon the inner surface of the airfoil leading edge or the slat (Fig. 2) in the case of a multi-element configuration. The inner region (region Ω in Fig. 2) is then modeled with a local internal convection coefficient h_{anti} which is considered to be known a priori. The heat flux q_{anti} coming from region Ω is then evaluated with the help of internal hot-air temperature T_{anti} and the local wall temperature T_w.

$$q_{\text{anti}} = h_{\text{anti}}(T_{\text{anti}} - T_w) \tag{1}$$

A limitation of this method is that the internal heat flux q_{anti} or the convection coefficient h_{anti} and temperature T_{anti} *are* based on empirical relations [6] for a hot-air jet impinging on a flat plate. This has been a commonly accepted practice in studies related to anti-icing system modeling [10–23]. It must be pointed out that this local distribution of internal heat flux q_{anti} or the convection coefficient h_{anti} is purely based on the local distribution on a flat plate and, therefore, does not account for the curvature of the internal wall region Ω of an airfoil leading edge or the wing slat. Another limitation of such a model is that it fails to provide an accurate estimate of the hot-air flux requirements and the drain on the engine power as a result of operating the hot-air anti-icing system. Moreover, it neither takes into account the hot-air heat flux lost to the atmosphere as some of the heat flux leaves the system through the exits, nor does it take into account the heat losses encountered in the ducts as the hot-air is forced from the engines to the piccolo tube.

To address these limitations, a more rigorous treatment of the internal hot-air region Ω is needed and an in-depth analysis of a hot-air anti-icing system becomes imperative. Use of computational fluid dynamics (CFD) tools to model the internal hot-air region in conjunction with a three-dimensional ice accretion code requires extensive computational resources and, therefore, these tools are not cost efficient to accomplish anti-icing simulation or optimum design of hot-air anti-icing systems for aircraft wings. One way to avoid such a large computational overhead and make the anti-icing simulation more efficient is to employ numerical correlations for the range of operation of the anti-icing system. Thus, these tools can be used to develop numerical correlations for internal heat transfer from a single jet or an array of hot-air jets impinging on the internal surface of a typical wing slat. Moreover, the numerical simulations could also be used to determine the effect of various important variables, such as jet nozzle-to-surface height, nozzle-to-nozzle spacing, spatial arrangement of hot-air jets, hot-air jet orientation, optimum height and spacing, etc., which can play an important role in the design of such systems.

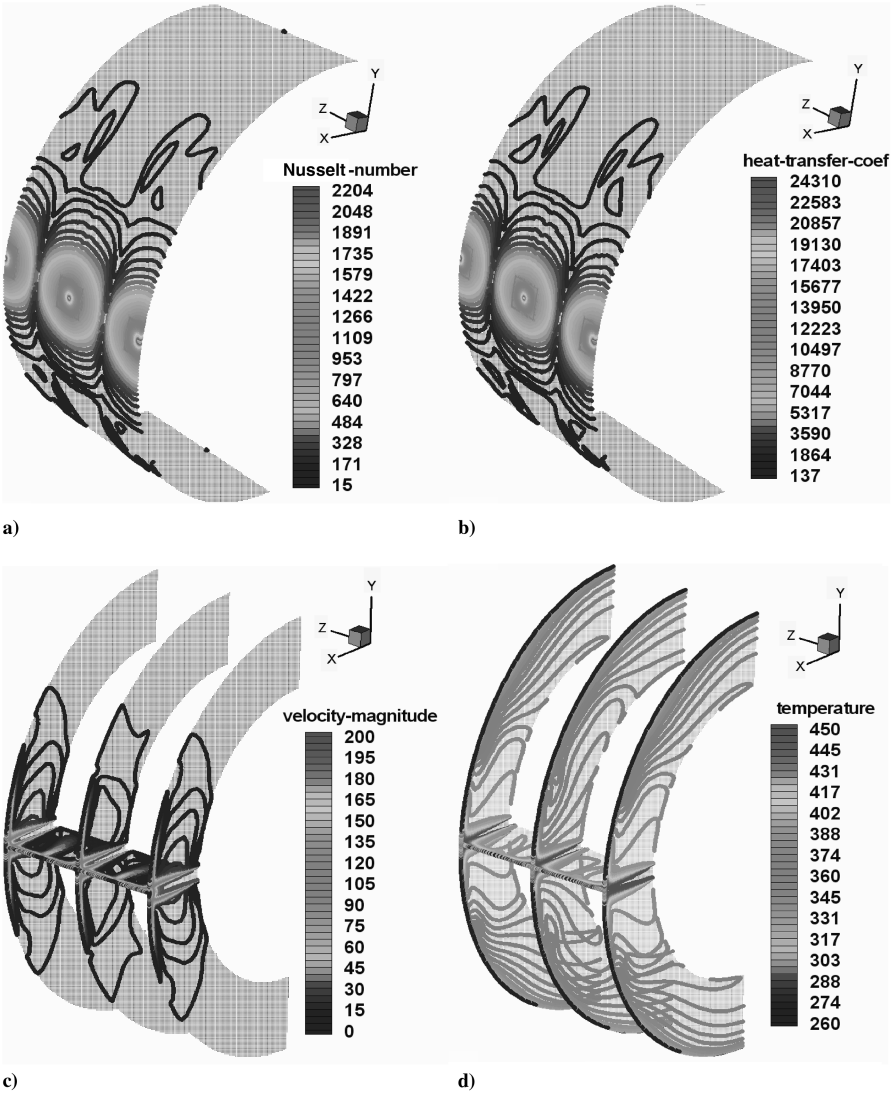

Fig. 8 Converged results for case 1: a) *Nu*, b) h_c, c) *T*, and d) *V* distributions.

The first step toward achieving an optimum design of a hot-air anti-icing system is the development of a reliable database, experimental and numerical, related to the heat transfer from single jet or an array of jets impinging on a curved surface. Recent studies [24,25] on the usefulness of the empirical relations developed for hot-air jet impingement on a flat surface for a highly curved, two-dimensional surface showed that the flat-plate empirical relations are inadequate for predicting heat transfer on curved surfaces. The aim of these studies was to determine numerical correlations for heat transfer on a two-dimensional, curved surface using state-of-the-art commercial CFD tools. Figures 3 and 4 present some results of the numerical simulation of a hot-air jet impingement on a concave surface for a two-dimensional case. As evident from Fig. 4, the most important conclusion drawn from these studies is that the flat-plate correlations are not reliable enough for predicting heat transfer on a concave surface.

As previously mentioned, these studies are of a two-dimensional nature, whereas the flow inside a slat is of a highly three-dimensional nature and, as such, cannot be represented by two-dimensional correlations, whether empirical of numerical. It is therefore imperative that a similar numerical study be undertaken to take into account the three-dimensional nature of the problem. The results of these three-dimensional experimental and numerical studies will be used to develop a three-dimensional aircraft anti-icing simulation code, which will not only aid aircraft manufacturers in certification of their aircraft for flight through natural icing conditions, but also help improve aircraft safety. Furthermore, the results will also aid in the design of an efficient anti-icing system through the development of a hot-air anti-icing system design and optimization tool. In view of these concerns, a recent study [26] examined the surface heat transfer from a single array of hot-air jets as a function of the jet height (jet-to-surface) and jet-to-jet spacing with varying jet Mach numbers. The study helped develop numerical heat-transfer correlations for a single array of hot-air jets impinging on a three-dimensional, concave surface simulating the inner surface of a slat.

Recently, research in this area has gained much interest. An evaluation of existing jet impingement heat-transfer correlations for piccolo tube applications was performed by Wright [27]. The study reviewed correlations by Martin [6], Hrycak [28], Gau and Chung [29], Tawfek [30,31], Goldstein and Sol [32], Goldstein et al. [33], Florschuetz et al. [34], Huber and Viskanta [35], and Huang and El-Genk [36]. The correlation of Goldstein et al. [33] was used to determine its usefulness. The study found that the correlation overpredicted surface temperature, resulting in a difference in predicted and experimental residual ice shapes. The study concluded that such a technique holds promise for rapidly obtaining first-order estimates of piccolo tube performance. Experimental and numerical parametric studies of a bleed air ice protection system were recently conducted by Papadakis and Wong [37] to investigate performance of an inner-bleed air anti-icing system typical of those found in regional and general aviation business jets. The study explored internal flow behavior and methods to enhance heat transfer to the wing skin (impingement wall). The conclusion of their investigation was that the skin temperatures for the inner liner bleed air system

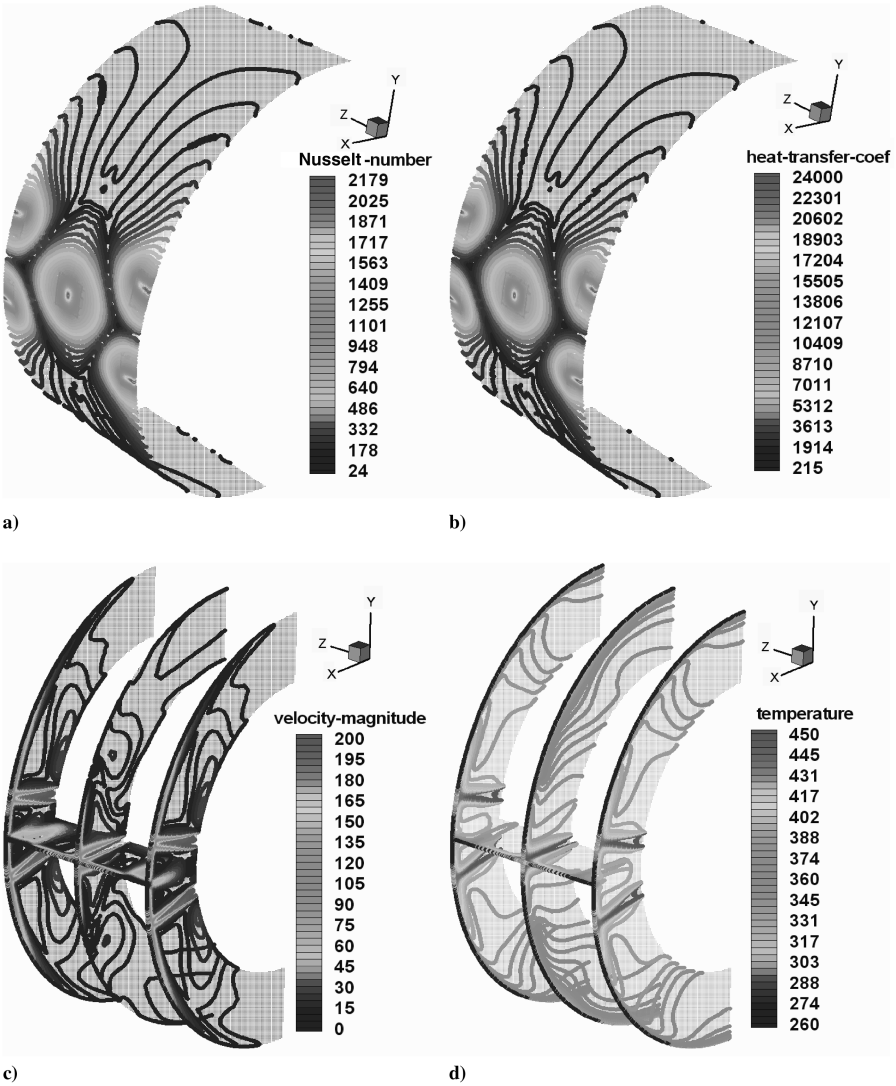

Fig. 9 Converged results for case 2: a) *Nu*, b) h_c, c) *T*, and d) *V* distributions.

were sensitive to piccolo tube location with respect to the wing leading edge (impingement wall) and the piccolo-hole pattern/arrangement.

Studies involving commercial or inhouse CFD codes, such as FENSEP/FENSEP-ICE [23,38], FLUENT [25,26,39–41], and PHOENICS [42,43], etc., have shown the usefulness of numerical simulations in assessing anti-ice heating requirements, as well as modeling and simulation to obtain better insight into the flow and heat-transfer characteristics of hot-air jets impingement. In light of this renewed interest in the subject, the current study was carried out to numerically simulate the heat transfer from an array of hot-air jets typical of those found in regional jet aircraft. Surface heat transfer from a staggered array of impinging hot-air jets or multiple jets at different orientation (angles) was numerically modeled using the commercially available CFD software, FLUENT. The objective of the current study was to examine the amount of heat transfer to the impingement surface (wing/slat skin) in relation to the amount of heat being supplied by the bleed air system, and also to the amount of heat lost as the hot-air exits the system. The effect of an etched channel or an inner liner (see Fig. 1) that confines the flow within a very narrow channel, or the use of baffles to confine the hot air in the vicinity of the leading edge, were also examined to get insight into ways and means to increase surface heat transfer through the impingement surface or to explore novel concepts that can lead to increased surface heat transfer. Thus, the different hot-air jet arrangements used in the numerical study include 1) an array of single jets, 2) an array of staggered jets (10 and 20 deg), and 3) an array of single jets and the use of baffles and etched channel/liner to enhance heat transfer through the outer surface, as depicted in Fig. 5. Figure 6 shows the different geometric parameters used in the study.

In the sections that follow, details of the CFD modeling is described first, followed by a section on the numerical results and the associated discussion. The paper ends with some brief conclusions.

II. Numerical Modeling using FLUENT

The commercial CFD software FLUENT [39] was used to model the flow in the internal hot-air region and conduct heat-transfer simulations. FLUENT uses a finite volume method to solve the Reynolds-averaged Navier–Stokes (RANS) equations which represent the governing equations for fluid flow. The RANS equations are simply the equations relating the conservation of mass, momentum, and energy. For turbulent flow simulations, additional transport equations are used to obtain a closed system of equations. For solid walls, such as the wing/slat surface or impingement wall, only the heat conduction through the wall is computed. The physical model of piccolo tube and associated geometry is modeled using GAMBIT [40]. GAMBIT is a geometry modeling and meshing tool associated with FLUENT. It is capable of generating structured, unstructured, and hybrid meshes in two- and three-dimensional domains. For this study, structured meshes involving hexahedral

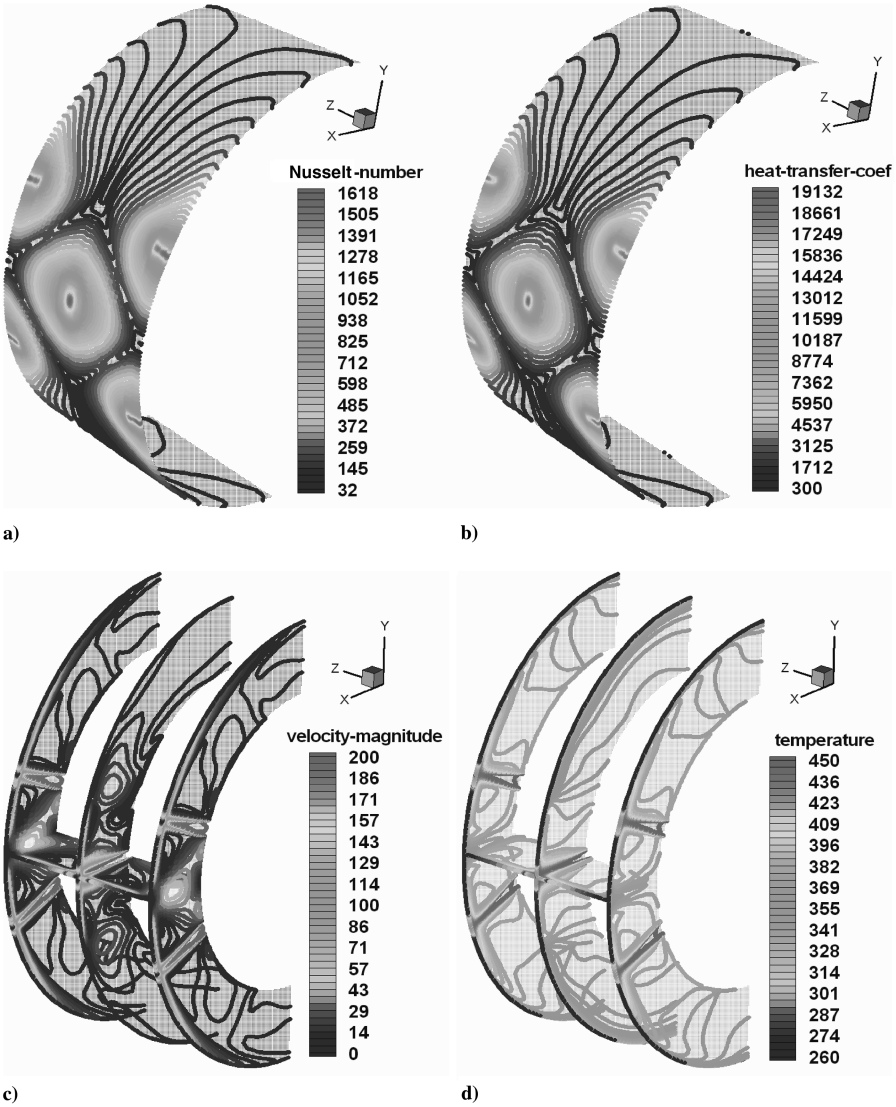

Fig. 10 Converged results for case 3: a) *Nu*, b) h_c, c) *T*, and d) *V* distributions.

elements were used to model the interior volumes of the wing model. Figure 7 shows the grid geometries used for the four different configurations: Fig. 7a in-line jets, Fig. 7b staggered jets (10 deg stagger), Fig. 7c staggered jets (20 deg stagger), and Fig. 7d in-line jets with a baffle and inner liner.

To accurately resolve flow and heat-transfer properties near the walls and in regions containing the hot-air jets, the grid density was appropriately chosen, as well as adapted, later. This choice was dictated by the recommendations for using nonequilibrium wall functions in complex flows involving separation, reattachment, and impingement for a more reliable prediction of wall shear (skin-friction coefficient) and heat transfer (Nusselt or Stanton number). Based on the recommendations in FLUENT, the wall-adjacent cell distance (cell center-to-wall distance) in terms of the nondimensional distance y^+ was kept on the order of one ($y^+ < 4$–5). Additional details of the different grids used in this study are given in the results and discussion section.

The realizable k-ε turbulence model was used in this study because it more accurately predicts the spreading rate of both planar and round jets compared with other turbulence models. Initially, the first-order upwind schemes were used in conjunction with relaxation factors between 0.4–0.7. After several thousand iterations, the second-order discretization schemes were employed. Two convergence criteria were used to monitor solution convergence. The first criterion was based on the residuals reaching a value of 10^{-6} or below. The second criterion was based on the net mass and heat flux values. It was observed that energy conservation requires substantial iterations (typically between 30,000–50,000 iterations) to converge. Typical grids were on the order of 0.6 to 1 million cells. Because of the coarse nature of initial grids, grid adaptation was typically carried out to achieve a value of y^+ below two or three (in most cases below two). Adapted grids typically consisted of approximately 20–30% more cells. On a 3 GHz, 2 GB RAM, desktop PC running Windows, it took about 4–6 days to converge to a solution.

No-slip boundary conditions were used at the walls. An isothermal (constant temperature of 260 K) wall boundary condition was set for the impingement wall with a thickness of 0.002 m and a thermal conductivity of 0.02 $\mathrm{W/m^2}$ (aluminum). Walls representing piccolo tube, baffle, and the liner (etched) surface were set with a zero heat flux boundary condition. Hot-air jet inlets were modeled using the velocity inlet boundary conditions where the velocity and temperature of the jet were specified. The flow exit was defined as an outflow boundary with a mass flow weighting of one. Reference values used in the study are as follows: $L_{\mathrm{ref}} = 0.0025$ m, $T_{\mathrm{ref}} = 288$ K, $V_{\mathrm{ref}} = 200$ m/s, $p_{\mathrm{ref}} = 0$ Pa, $\rho_{\mathrm{air}} = 1.225$ $\mathrm{kg/m^3}$, and $\mu_{\mathrm{air}} = 1.789\mathrm{E}-05$ $\mathrm{kg/m \cdot s}$.

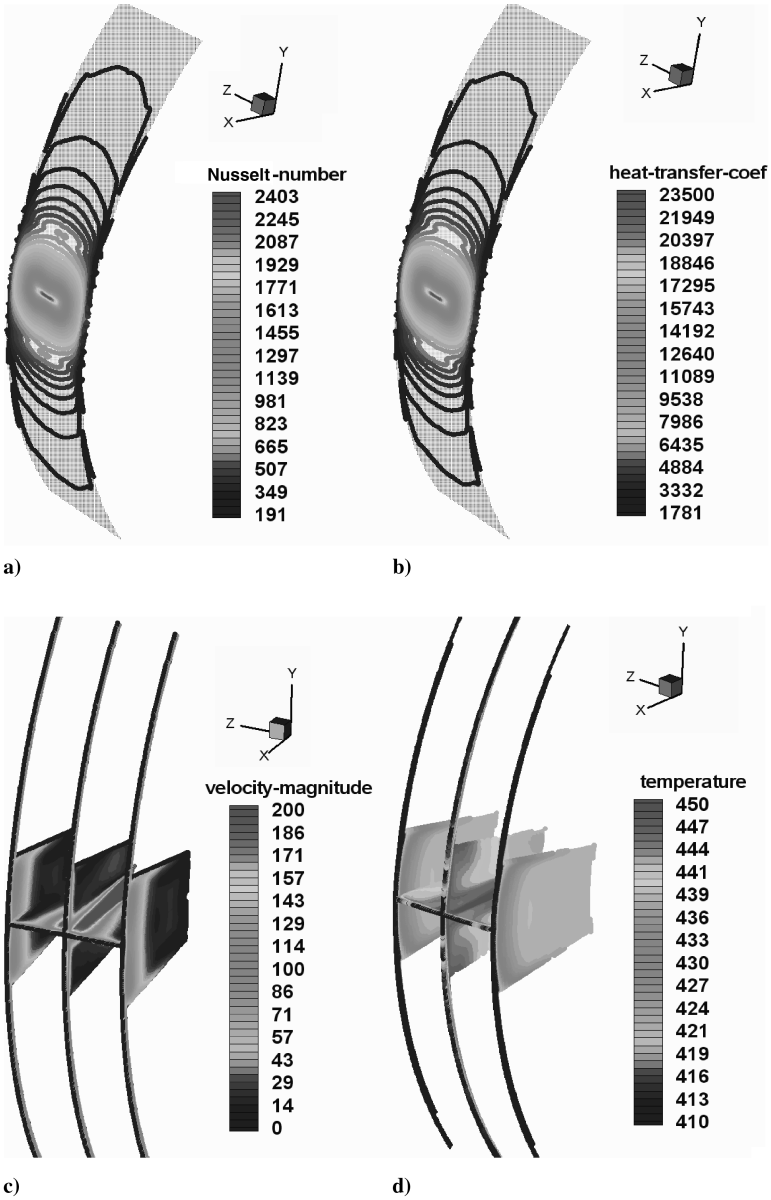

Fig. 11 Converged results for case 14: a) Nu, b) h_c, c) T, and d) V distributions.

It is noted here that the current study is an extension of the work reported in [25,26], in which the validity of the numerical model was shown by comparison with the empirical data of Gardon and Cobonpue [44] for jets (three-dimensional) impinging on a flat wall. The reader should refer to [25,26] for details on the validity of the model.

III. Results and Discussion

Table 1 lists the description of various numerical simulations covered in this study. The mass flow and heat-transfer rates for each of the cases is listed in Table 2. Table 3 lists a summary of the percentage distribution of the heat transfer through the impingement wall q_w, as well as the heat flux lost through the exit q_{out}. It is worth noting that the impingement surface areas are different for the single/liner cases than the rest by a factor of seven. Hence, an area-weighted average of the total surface heat flux was calculated for all cases and is listed in the second-to-last column of Table 3. Because the mass and heat influx between the single array and the staggered array differ by a factor of 1.5, the same scale factor was used to correct the area-weighted average for the difference in the mass and heat influx. A comparison of the area-weighted average of the total surface heat flux of the different cases reveals that a 20 deg stagger does help increase heat transfer through the impingement surface, whereas 10 deg does not. An immediate explanation for this is yet not known but it certainly requires further investigation. It is quite possible that an optimum stagger angle may yield a maximum value of surface heat flux. Examining the last five cases of the inner liner, the corrected area-weighted average reveals surface heat flux values almost 2–3 times higher than the corresponding single array case. This verifies the usefulness of incorporating a liner or an etched surface in the design of the wing leading edge to enhance the surface heat-transfer mechanism.

Figure 7 shows the grid geometry for the different configurations: Fig. 7a in-line, Fig. 7b staggered (10 deg stagger between the two jet holes), Fig. 7c staggered (20 deg stagger), and Fig. 7d in-line with baffle and inner liner or etched surface. Difference between the original (Fig. 7c) and refined (Figs. 7a and 7b) grids can be inferred by comparing the piccolo tube and the impingement surfaces in the figure. The left, right, and bottom faces of the mesh represent the symmetry boundaries of the computational domain. In Fig. 7d, a baffle and an inner liner/etched surface is introduced to channel the

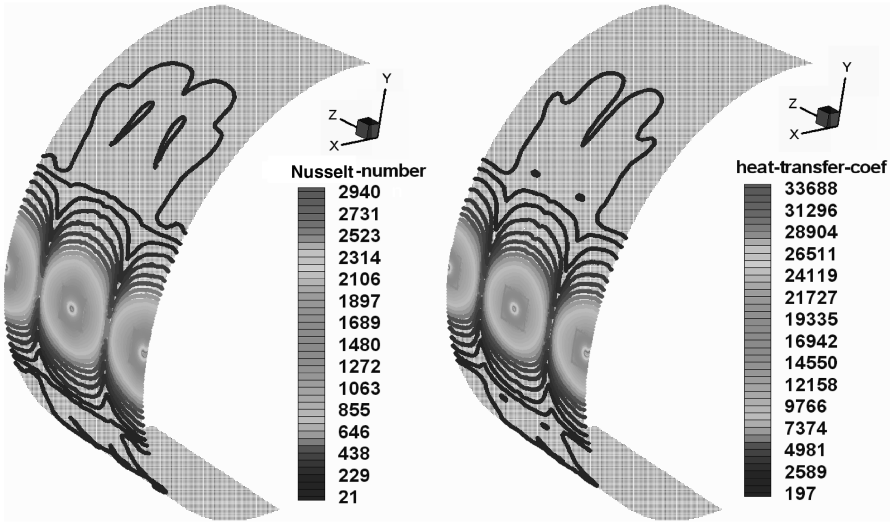

a) b)

Fig. 12 Converged results for case 4: a) *Nu* and b) h_c distributions.

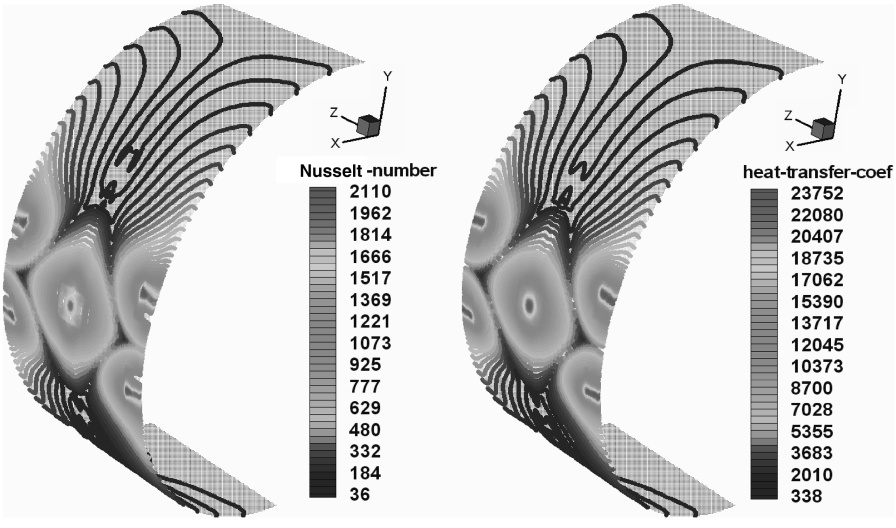

a) b)

Fig. 13 Converged results for case 5: a) *Nu* and b) h_c distributions.

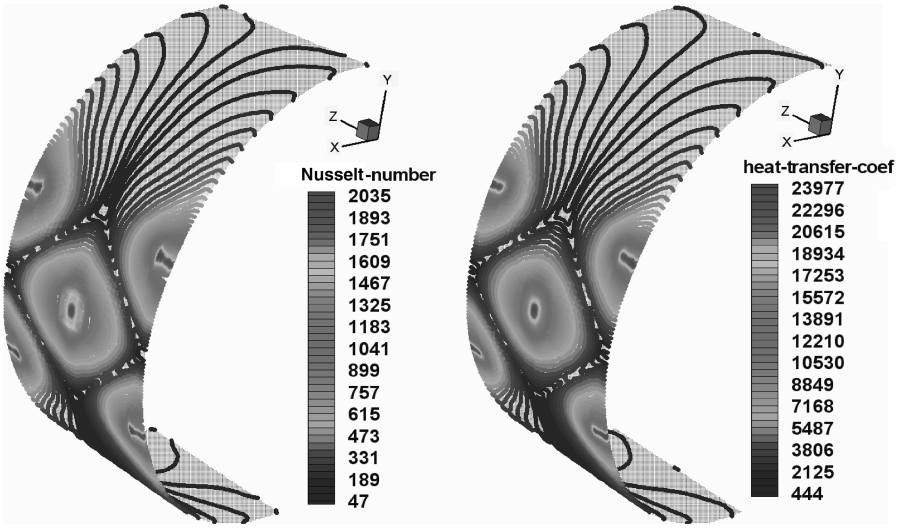

a) b)

Fig. 14 Converged results for case 6: a) *Nu* and b) h_c distributions.

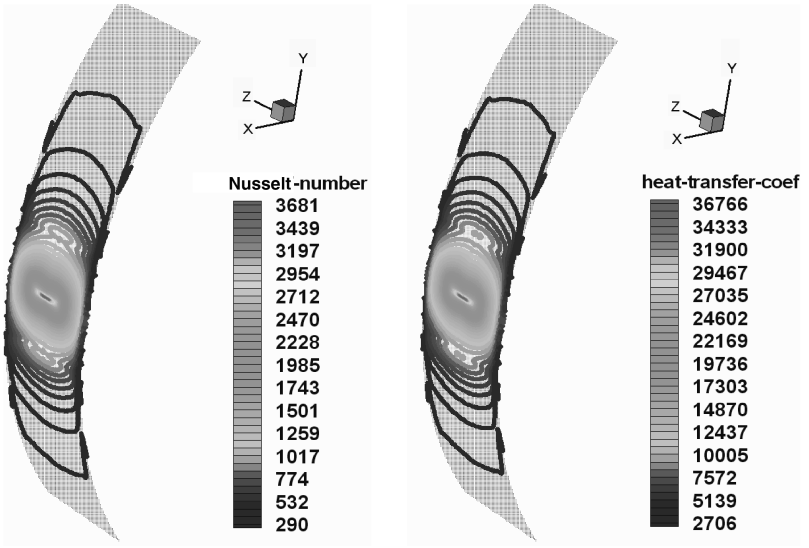

a) b)

Fig. 15 Converged results for case 15: a) *Nu* and b) h_c distributions.

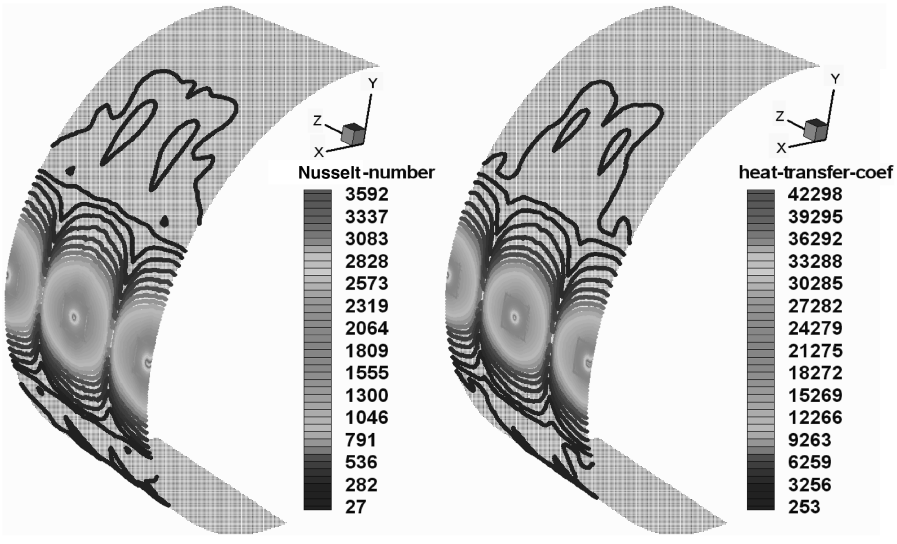

a) b)

Fig. 16 Converged results for case 7: a) *Nu* and b) h_c distributions.

flow through a very narrow passage along the impingement surface. Because FLUENT does not have a three-dimensional boundary-layer analysis capability, the narrow channel was modeled in terms of straight channel segments at 5 deg intervals. The height (gap) of the channel was selected such that the height is more than twice the wall boundary-layer thickness. For meshing the channels, the wall-adjacent cell height y^+ was kept to the order of one.

Figures 8–11 show the converged results in terms of Nu, h_c, V, and T distributions for cases 1, 2, 3, and 14, where $V_{\text{jet}} = 200$ m/s and $T_{\text{jet}} = 450$ K. The first values in the legend of all the contour plots in the study represent the maximum value of that variable. Figures 12–25 show the converged results for Nu and h_c distributions for the rest of the cases. Results for the in-line jets show very high heat transfer at the stagnation region on the impingement surface that drops off sharply in the vicinity of the stagnation region. The stagnation region for the staggered jets cases is more elongated, in general, and curved in the direction of the flow, in particular, for the jets impinging away from the centerline and is a result of the presence of crossflow. The stagger also results in a higher surface heat transfer as a result of larger surface coverage and lesser heat loss through the exit. The stagnation region for the inner liner/etched surface case is also elongated. Moreover, an increase in surface heat transfer results at the start of the channel due to acceleration of the flow as it enters the confined channel. Figure 26 shows a comparison of area-weighted total surface heat transfers from the different models and clearly shows the advantage of using an inner liner/etched surface for increased surface heat transfer.

IV. Conclusions

This study was conducted to numerically simulate the heat transfer from an array of jets onto an impingement surface. The study used the commercially available CFD software, FLUENT, to model the different hot-jet arrangements that included 1) a single array of jets, 2) two staggered arrays of jets at different stagger angles (10 and 20 deg), and 3) a case with an etched surface. The main findings of the study reveal that the single array and the array with a 20 deg stagger yield better surface heat transfer than the 10 deg stagger. The etched surface yields almost 2–3 times better surface heat transfer than the rest, making it a favorable choice for increasing heat transfer. Further studies need to be conducted to determine the optimum stagger as well as the channel location and height (gap) to maximize surface

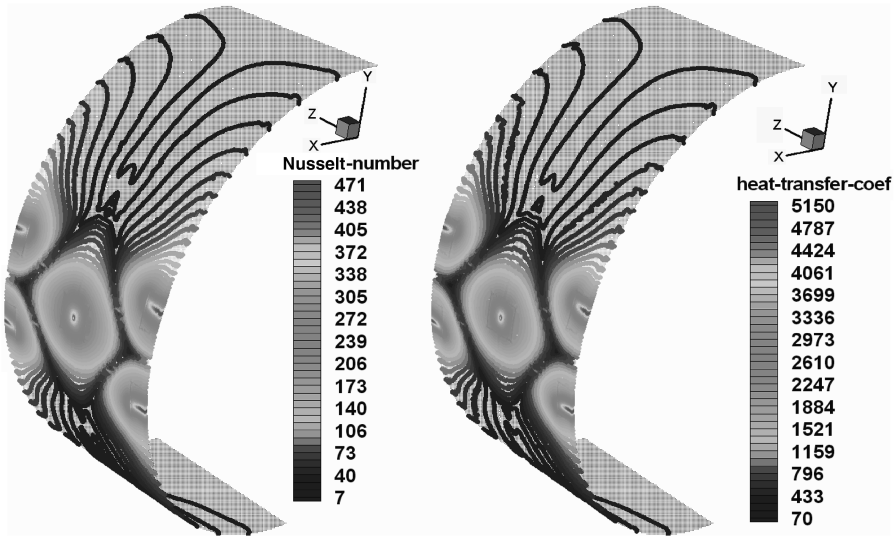

a) b)

Fig. 17 Converged results for case 8: a) Nu and b) h_c distributions.

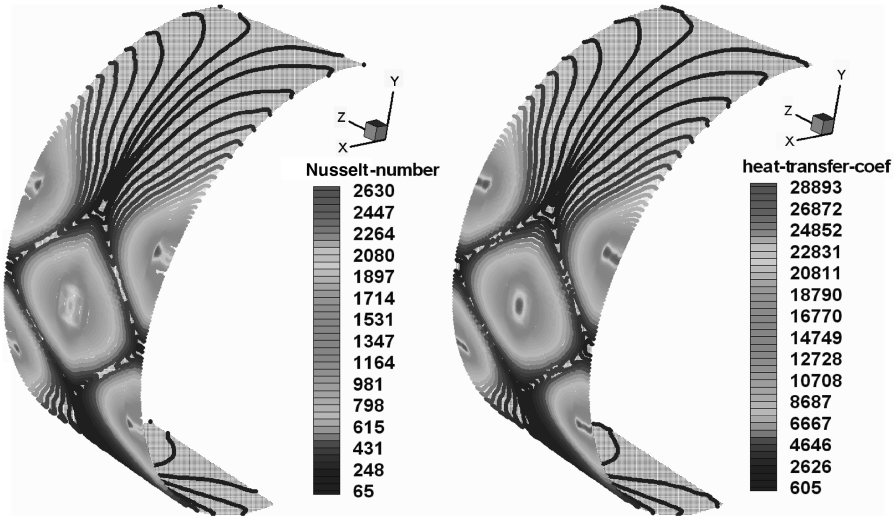

a) b)

Fig. 18 Converged results for case 9: a) Nu and b) h_c distributions.

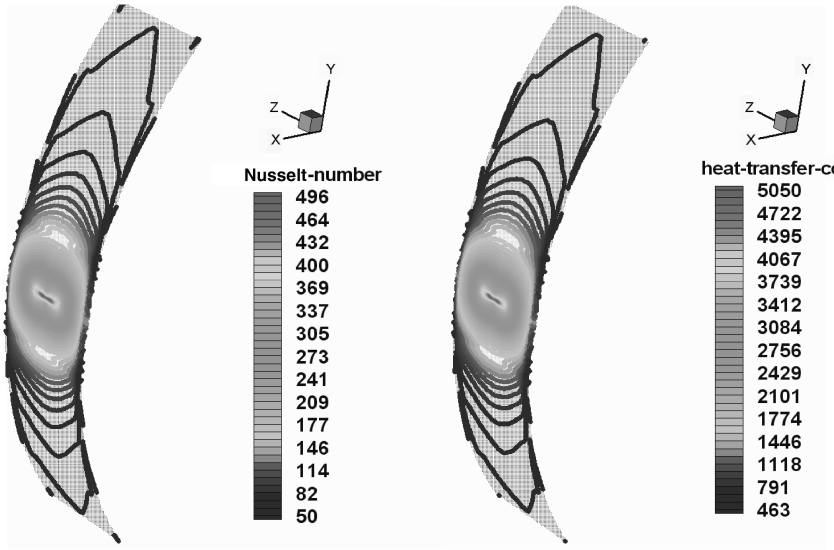

a) b)

Fig. 19 Converged results for case 16: a) *Nu* and b) h_c distributions.

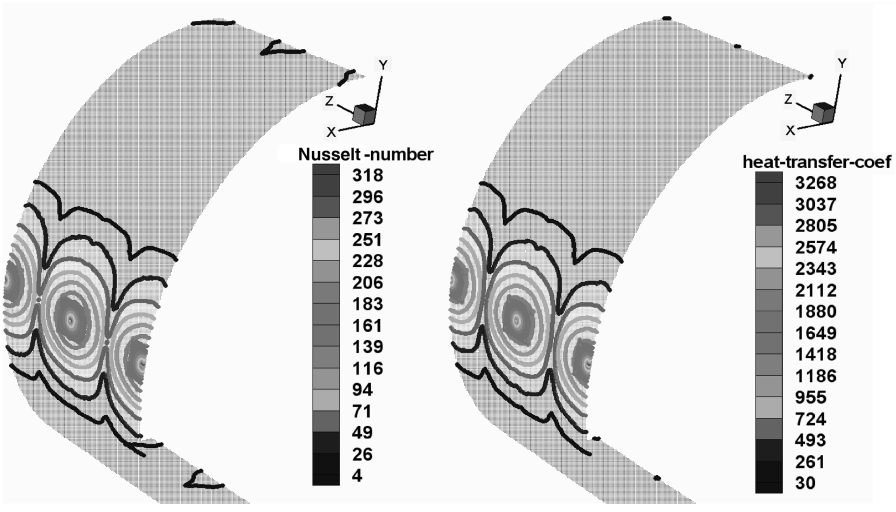

a) b)

Fig. 20 Converged results for case 10: (a) *Nu* and (b) h_c distributions.

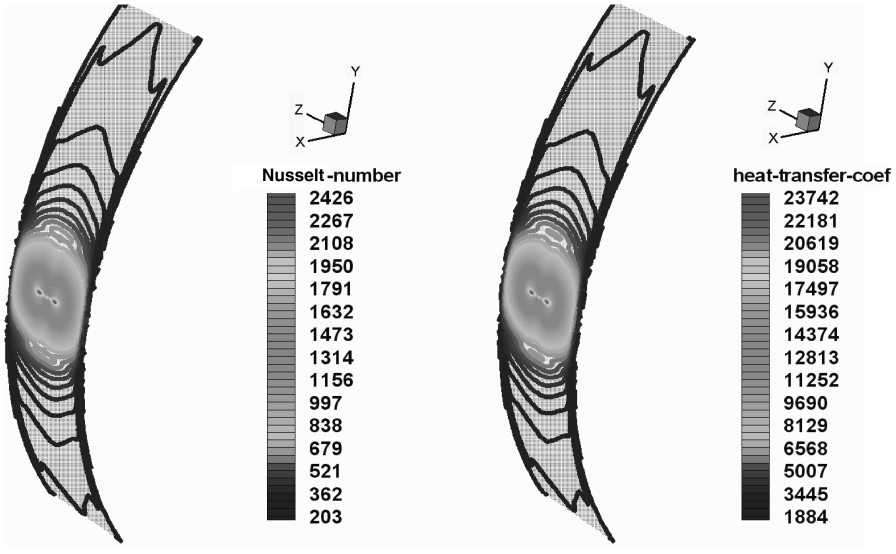

a) b)

Fig. 21 Converged results for case 17: a) *Nu* and b) h_c distributions.

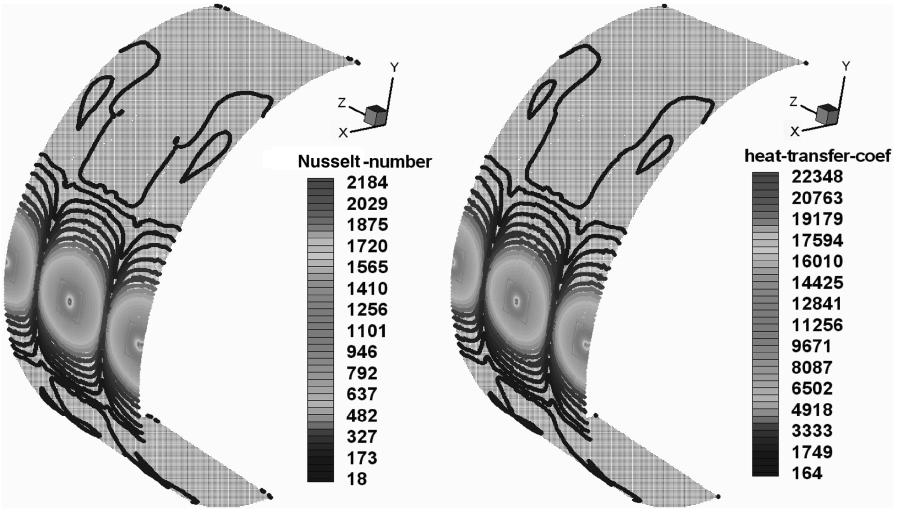

a) b)

Fig. 22 Converged results for case 11: a) *Nu* and b) h_c distributions.

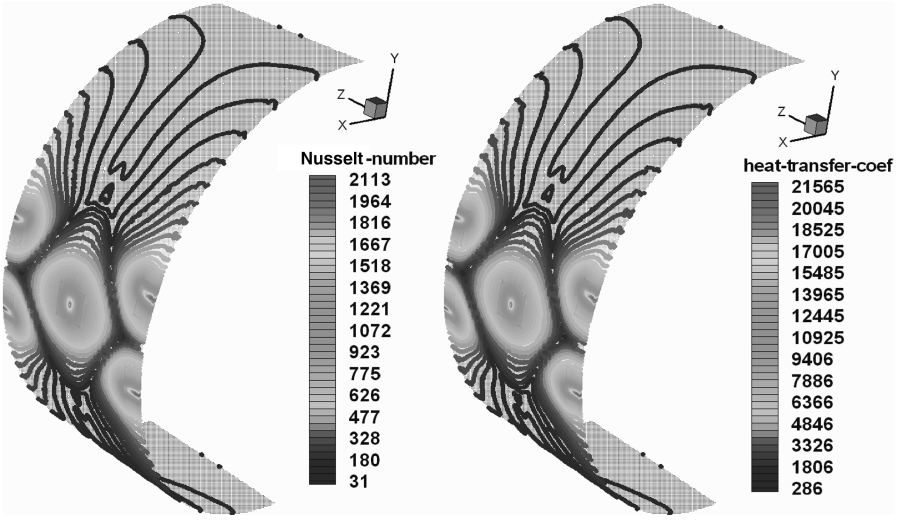

a) b)

Fig. 23 Converged results for case 12: a) *Nu* and b) h_c distributions.

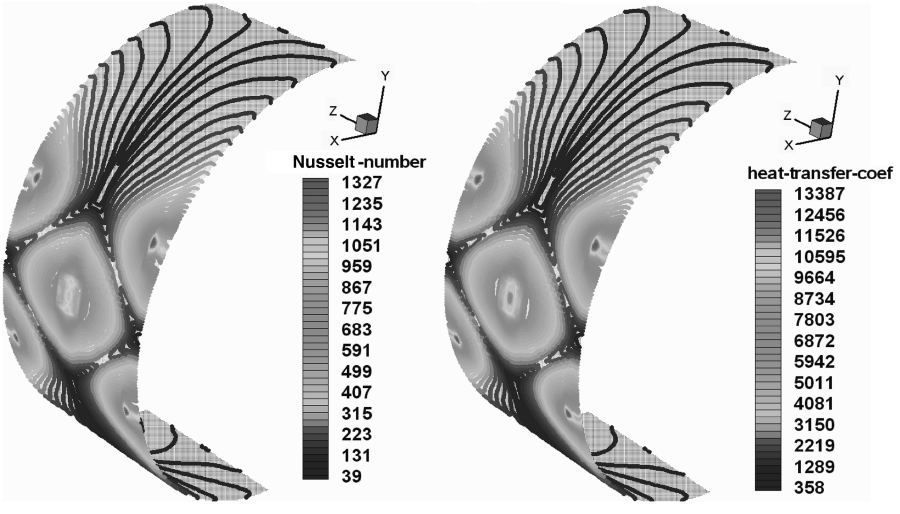

a) b)

Fig. 24 Converged results for case 13: a) *Nu* and b) h_c distributions.

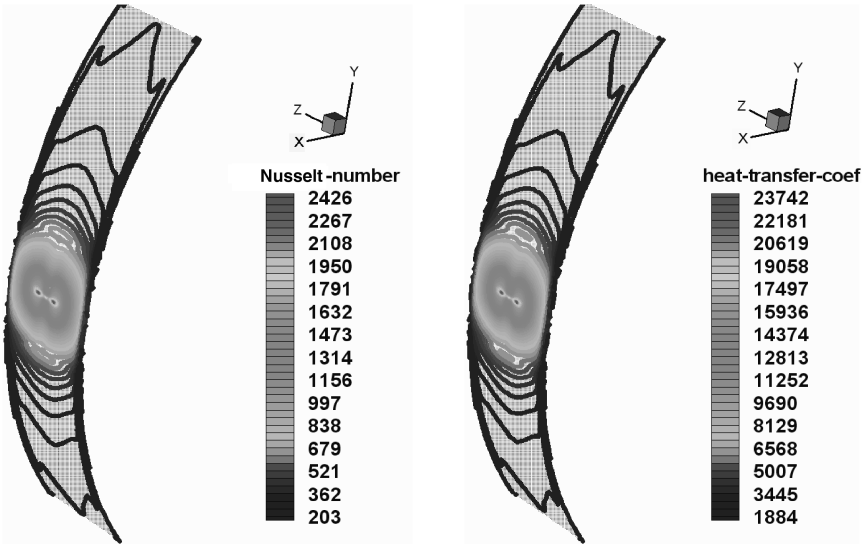

a) b)

Fig. 25 Converged results for case 18: a) *Nu* and b) h_c distributions.

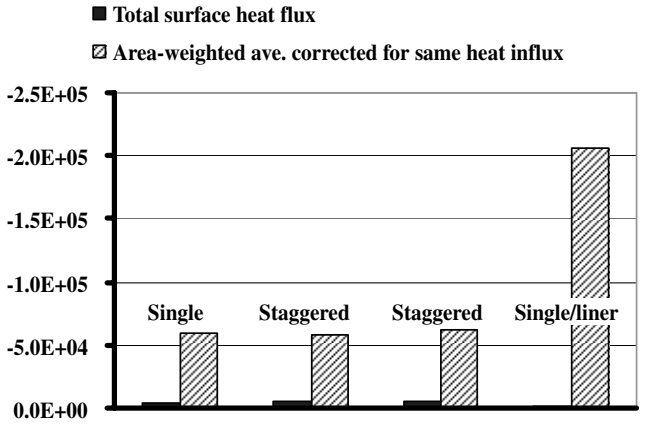

Fig. 26 Comparison of area-weighted total surface heat transfers from the different models.

heat transfer. A significant amount of heat is also lost via the exit. Means to rechannel or use the hot-air exiting the system need to be examined to make the system more efficient. Because the surface heat transfer drops off sharply in the vicinity of the stagnation point, means and ways to extend the region need to be explored as well to make it more efficient.

Acknowledgments

The work in this study was supported by the grant for the fast track project FT-2005/04 by the Deanship of Scientific Research, King Fahd University of Petroleum and Minerals, Dhahran, Saudi Arabia. The authors are grateful for the aforementioned support in accomplishing this study. The authors would also like to acknowledge helpful discussions with Ion Paraschivoiu and Octavian Trifu, Ecole Polytechnique de Montreal, and Fassi Kafeke, Bombardier Aerospace, Montreal, Canada.

References

[1] Federal Aviation Administration, *Proceedings of the FAA International Conference on Aircraft In-Flight Icing*, Vols. 1–2, Federal Aviation Adminstration, Washington, D.C., May 1996 Final Report.

[2] FAA In-Flight Icing Plan, U.S. Dept. of Transportation, Federal Aviation Administration, April 1997.

[3] Thomas, S. K., Cassoni, R. P., and MacArthur, C. D., "Aircraft Anti-Icing and Deicing Techniques and Modeling," *Journal of Aircraft*, Vol. 33, No. 5, Sept.–Oct. 1996, pp. 841–854.

[4] Brown, J. M., Raghunathan, S., Watterson, J. K., Linton, A. J., and Riordon, D., "Heat Transfer Correlation for Anti-Icing Systems," *Journal of Aircraft*, Vol. 39, No. 1, Jan.–Feb. 2002, pp. 65–70.

[5] Jambunathan, K., Lai, E., Moss, M. A., and Button, B. L., "Review of Heat Transfer Data for Singular Jet Impingement," *International Journal of Heat and Fluid Flow*, Vol. 13, No. 2, 1992, pp. 106–115. doi:10.1016/0142-727X(92)90017-4

[6] Martin, H., "Heat and Mass Transfer Between Impinging Gas Jets and Solid Surfaces," *Advances in Heat Transfer*, Vol. 13, Academic Press, New York, 1977, pp. 1–60.

[7] Cornaro, C., Fleischer, A. S., and Goldstein, R. J., "Flow Visualisation of a Round Jet Impinging on Cylindrical Surfaces," *Experimental Thermal and Fluid Science*, Vol. 20, No. 2, 1999, pp. 66–78. doi:10.1016/S0894-1777(99)00032-1

[8] Metzger, D. E., Yamashita, T., and Jenkins, C. W., "Impingement Cooling of Concave Surfaces with High Velocity Impinging Air Jets," *Journal of Engineering for Power*, Vol. 91, 1969, pp. 149–158.

[9] Dyban, E. P., and Mazur, A. I., "Heat Transfer for a Planar Jet Striking a Concave Surface," Translated from *Inzhenerno-Fizicheskii Zhurnal*, Vol. 17, No. 5, Nov. 1969, pp. 785–790.

[10] Morency, F., Tezok, F., and Paraschivoiu, I., "Anti-Icing System Simulation Using CANICE," *Journal of Aircraft*, Vol. 36, No. 6, Nov.–Dec. 1999, pp. 999–1006.

[11] Morency, F., Tezok, F., and Paraschivoiu, I., "Heat and Mass Transfer in the Case of an Anti-Icing System Modelisation," *Journal of Aircraft*, Vol. 37, No. 2, Mar.–Apr. 2000, pp. 245–252; also AIAA Paper 99-0623, Jan. 1999.

[12] Morency, F., Tessier, P., Saeed, F., and Paraschivoiu, I., "Anti-Icing System Simulation on Multielement Airfoil," *CASI 46th Annual Conference/DNP-ASIP*, Canadian Aeronautics and Space Inst., Kanata, Ontario, Canada, May 1999, pp. 463–470.

[13] Tran, P., Brahimi, M. T., Sankar, L. N., and Paraschivoiu, I., "Ice Accretion Prediction on Single and Multi-Element Airfoils and the Resulting Performance Degradation," AIAA Paper 97-0178, Jan. 1997.

[14] Tran, P., Brahimi, M. T., Paraschivoiu, I., Pueyo, A., and Tezok, F., "Ice Accretion on Aircraft Wings with Thermodynamic Effects," *Journal of Aircraft*, Vol. 32, No. 2, 1995, pp. 444–446.

[15] Paraschivoiu, I., Tran, P., and Brahimi, M. T., "Prediction of the Ice Accretion with Viscous Effects on Aircraft Wings," *Journal of Aircraft*, Vol. 31, No. 4, July–Aug. 1994, pp. 855–861.

[16] Tran, P., Brahimi, M. T., and Paraschivoiu, I., "Ice Accretion on Aircraft Wings," *Canadian Aeronautics and Space Journal*, Vol. 40, No. 3, Sept. 1994, pp. 185–192.

[17] Ruff, G. A., and Berkowitz, B. M., "User Manual for the NASA Lewis Ice Accretion Code Prediction Code LEWICE," NASA, CR 185129, May 1990.

[18] Wright, W. B., "User Manual for the Improved NASA Lewis Ice Accretion Code LEWICE 1.6," NASA, CR 198355, June 1995.

[19] Al-Khalil, K. M., "Numerical Simulation of an Aircraft Anti-Icing System Incorporating a Rivulet Model for the Runback Water," Ph.D. Thesis, Univ. of Toledo, Toledo, OH, June 1991.

[20] Al-Khalil, K. M., and Potapczuk, M. G., "Numerical Modeling of Anti-Icing Systems and Numerical Comparison to Test Results on a NACA 0012 Airfoil," *31st Aerospace Sciences Meeting and Exhibit*, AIAA Paper 93-0170, Jan. 1993.

[21] Al-Khalil, K. M., Ferguson, T. W., and Phillips, D. M., "Hybrid Anti-Icing Ice Protection System," *35th Aerospace Science Meeting and Exhibit*, AIAA Paper 97-0302, Jan. 1997.

[22] Meola, C., Carlomagno, G. M., Riegel, E., and Salvato, F., "Experimental Study of an Anti-Icing Hot Air Spray-Tube System," *19th Congress ICAS*, International Council of the Aeronautical Sciences, Stockholm, 1994.

[23] Croce, G., Habashi, W. G., Guévremont, G., and Tezok, F., "3D Thermal Analysis of an Anti-Icing Device Using FENSAP-ICE," *36th Aerospace Sciences Meeting and Exhibit*, AIAA Paper 98-0198, Jan. 1998.

[24] Saeed, F., Morency, F., and Paraschivoiu, I., "Numerical Simulation of a Hot-Air Anti-Icing Simulation," *38th Aerospace Sciences Meeting and Exhibit*, AIAA Paper 2000-0630, Jan. 2000.

[25] Saeed, F., and Paraschivoiu, I., "Numerical Correlation for Local Nusselt Number Distribution for Hot-Air Jet Impingement on Concave Surfaces," *Proceedings of the 8th Annual Conference of the CFD Society of Canada, CFD2K*, Vol. 2, Taylor and Francis, London, June 2000, pp. 897–904.

[26] Fregeau, M., Saeed, F., and Paraschivoiu, I., "Numerical Heat Transfer Correlation for Array of Hot-Air Jets Impinging on 3-Dimensional Concave Surface," *Journal of Aircraft*, Vol. 42, No. 3, 2005, pp. 665–670.

[27] Wright, W. B., "Evaluation of Jet Impingement Heat Transfer Correlations for Piccolo Tube Application," NASA CR 212917, April 2004; also AIAA Paper 2004-0062, Jan. 2004.

[28] Hrycak, P., "Heat Transfer from a Row of Impinging Jets to Concave Cylindrical Surfaces," *International Journal of Heat and Mass Transfer*, Vol. 24, No. 3, Mar. 1981, pp. 407–419. doi:10.1016/0017-9310(81)90048-X

[29] Gau, C., and Chung, C. M., "Surface Curvature Effect on Slot-Air-Jet Impingement Cooling Flow and Heat Transfer Process," *Journal of Heat Transfer*, Vol. 113, Nov. 1991, pp. 858–864.

[30] Tawfek, A. A., "Heat Transfer Studies of the Oblique Impingement of Round Jets upon a Curved Surface," *Heat and Mass Transfer*, Vol. 38, No. 6, 2002, pp. 467–475. doi:10.1007/s002310100221

[31] Tawfek, A. A., "Heat Transfer and Pressure Distributions of an Impinging Jet on a Flat Surface," *Heat and Mass Transfer*, Vol. 32, Nos. 1–2, Nov. 1996, pp. 49–54. doi:10.1007/s002310050090

[32] Goldstein, R. J., and Sol, W. S., "Heat Transfer to a Row of Impinging Circular Air Jets Including the Effect of Entrainment," *International Journal of Heat and Mass Transfer*, Vol. 34, No. 8, 1991, pp. 2133–2147. doi:10.1016/0017-9310(91)90223-2

[33] Goldstein, R. J., Behbahni, A. I., and Heppelman, K. K., "Streamwise Distribution of the Recovery Factor and the Local Heat Transfer Coefficient to an Impinging Circular Air Jet," *International Journal of Heat and Mass Transfer*, Vol. 29, No. 8, 1986, pp. 1227–1235. doi:10.1016/0017-9310(86)90155-9

[34] Florshuetz, L. W., Metzger, D. E., and Truman, C. R., "Jet Array Impingement with Crossflow: Correlation of Streamwise Resolved Flow and Heat Transfer Distributions," NASA CR-3373, Jan. 1981.

[35] Huber, A. M., and Viskanta, R., "Effect of Jet-Jet Spacing on Convective Heat Transfer to Confined, Impinging Arrays of Axisymmetric Air Jets," *International Journal of Heat and Mass Transfer*, Vol. 37, No. 18, 1994, pp. 2859–2869. doi:10.1016/0017-9310(94)90340-9

[36] Huang, L., and El-Genk, M. S., "Heat Transfer of an Impinging Jet on a Flat Surface," *International Journal of Heat and Mass Transfer*, Vol. 37, No. 13, 1994, pp. 1915–1923. doi:10.1016/0017-9310(94)90331-X

[37] Papadakis, M., and Wong, S. J., "Parametric Investigation of a Bleed Air Ice Protection System," AIAA Paper 2006-1013, Jan. 2006.

[38] Croce, G., Beaugendre, H., and Habashi, W. G., "CHT3D: FENSAP-ICE Conjugate Heat Transfer Computations with Droplet Impingement and Runback Effects," AIAA Paper 20-0386, 2002.

[39] FLUENT 6 User's Guide, Fluent, Lebanon, NH, 2002, http://www.fluent.com (retrieved 6 Jan. 2008).

[40] GAMBIT 2 User's Guide, Fluent, Lebanon, NH, 2002, http://www.fluent.com (retrieved 6 Jan. 2008).

[41] Mattos, B. S., and Oliveria, G. L., "Three-Dimensional Thermal Coupled Analysis of a Wing Slice Slat with a Piccolo Tube," AIAA Paper 2000-3921, 2000.

[42] Smith, A. G., and Taylor, K., "Simulation of an Aircraft Engine Intake Anti-Icing System," *PHOENICS Journal of Computational Fluid Dynamics and Its Applications*, Vol. 10, No. 2, April 1997, pp. 150–166.

[43] PHOENICS CFD code, PHOENICS, Cham, England, 2000, http://www.simuserve.com/cfd-shop/index.htm (retrieved 6 Jan. 2008).

[44] Gardon, R., and Cobonpue, J., "Heat Transfer Between a Flat Plate and Jets of Air Impinging on It," *International Developments in Heat Transfer*, American Society of Mechanical Engineers, New York, Pt. 2, 1961, pp. 454–460.